Optimization and Numerical Investigation of Micro-pin-Fin Structure on Heat Sink with Checkerboard Nozzles

Huajie Lv, Kehan He, and Xing Ju(✉)

School of Energy, Power and Mechanical Engineering, North China Electric Power University, Beijing 102206, People's Republic of China
scottju@ncepu.edu.cn

Abstract. The micro-pin-fin heat sink with checkerboard nozzles has shown its ultra-high flux heat transfer capability, which has the potential to solve the critical problem for VLSI technology. In this paper, a numerical simulation analysis is carried out on the morphologic design, geometric parameters, and operating conditions. The calculation models on the cylinder, cone, round table, and bullet micro-pin-fins are established. The heat transfer performance of each morphologic structure is analyzed. The calculation results show that the pressure drop of the morphologic structure of the cylinder is small, but the eddy current also limits the heat transfer effect. It has obvious advantages when the truncated cone morphology is applied to the heat exchange unit. The pressure drop is only 5011.26 Pa, while the thermal resistance can be as low as 1.39×10^{-5} Km^2/W.

Keywords: Micro-Pin-Fin · Ultra-high heat flux · Nozzle jet

1 Introduction

With the continuous development of electronic chips, the production of chips with higher precision and higher integration has become the focus of global development. With the continuous improvement of transistor integration, the thermal density of high-speed electronic devices has reached 5 ~ 10 MW/m^2 [1], and heat dissipation has become the main problem to be solved in its development. It has become an inevitable trend for microchannel heat exchangers to replace traditional heat exchange devices. Common cooling techniques include heat pipe cooling [2], phase change cooling [3], single-phase air cooling and liquid cooling [4], nozzle jets [5], and microchannels [6]. Among them, micro-channel heat dissipation is more suitable for micro-scale chips, which complements its advantages of energy saving, excellent heat transfer performance, and broad research potential.

Y. Wang et al. (Eds.): ICSINC 2022, LNEE 996, pp. 146–154, 2023.
https://doi.org/10.1007/978-981-19-9968-0_18

However, the thermal boundary layer will gradually thicken after the fluid flows too long along the microchannels [7], significantly affecting heat transfer. With the development of the research on the heat sink structure, the micro-pin-fin with checkerboard nozzles has been verified as a potential heat transfer structure. Ju et al. [8] adopted a checkerboard nozzle-jet/manifold/micro-pin-fin composite heat sink. Shi et al. [9] proved that the square topology with a cylindrical pin-fin structure has better heat transfer performance by changing the nozzle distribution in the heat sink structure.

However, there is still a problem if the morphologic design of micro-pin-fins influences the heat sink performance. Although the morphologic design is discussed in many papers concerning micro-pin-fin heat sinks, it is totally different when the micro-pin-fins are under the array of impinging jets. Based on the micro-pin-fin structure with square cross-sections, the heat transfer unit of the cylindrical, conical, truncated, and bullet micro-pin-fins are simulated. The geometric and operating parameters are analyzed to achieve better thermal and hydrodynamic performance.

2 Geometric and Numerical Models

2.1 Geometric Model

Four different morphologies are proposed based on the different micro-pin-fin shapes in the vertical direction, as shown in Fig. 1. Among them, each micro-pin-fin is of the same height and volume. Different models were established by changing the shape of micro-pin-fins on the longitudinal section. Thus the thermal and hydrodynamic performances are explored as follows.

Case1: cylindrical pin-fin structure
Case2: conical pin-fin structure
Case3: circular truncated pin-fin structure
Case4: the bullet-shaped pin-fin structure is a rotating body of the power function $y = ax^2$.

In order to facilitate the comparative analysis of heat exchange structures with similar morphologies, the same element model is used for division. The unit model height H_{tot} of the basic example is 750 μm, which is composed of the base layer H_b, the micro-pin-fin layer H_{pf}, the cover layer H_C and the nozzle layer H_n. The following formula can obtain:

$$H_{tot} = H_b + H_{pf} + H_c + H_n \tag{1}$$

Table 1 shows the geometric parameters and operating conditions of the basic model.

Table 1. Basic geometric parameters and operating conditions of four different models.

Geometric parameters	Symbol	Case A	Case B	Case C	Case D
Heat sink width (cm)	W_{chip}	2	2	2	2
Substrate height (μm)	H_b	100	100	100	100
Cover height (μm)	H_c	100	100	100	100
Micro-pin-fin shape	Q	Cylinder	Conical	Truncated	Bullet
Micro-pin-fin bottom diameter (μm)	D_{pf}	86.6	150	122.48	122.48
Micro-pin-fin height (μm)	H_{pf}	250	250	250	250
Micro-pin-fin volume (μm^3)	V_{pf}	1472535	1472622	1472604	1472754
Nozzle diameter (μm)	D_n	50	50	50	50
Inlet velocity (m/s)	v_{in}	0.75	0.75	0.75	0.75
Inlet temperature (K)	T_{in}	293.15	293.15	293.15	293.15

2.2 Numerical Models

2.2.1 Unit Model

The morphology design of the heat exchange unit is repeatable on the two-dimensional plane, and this paper is applied to the heat sink of 2 cm*2 cm to dissipate heat. Rectangular columnar units are used, and each unit is a rectangular columnar model of 110 μm*110 μm*750 μm.

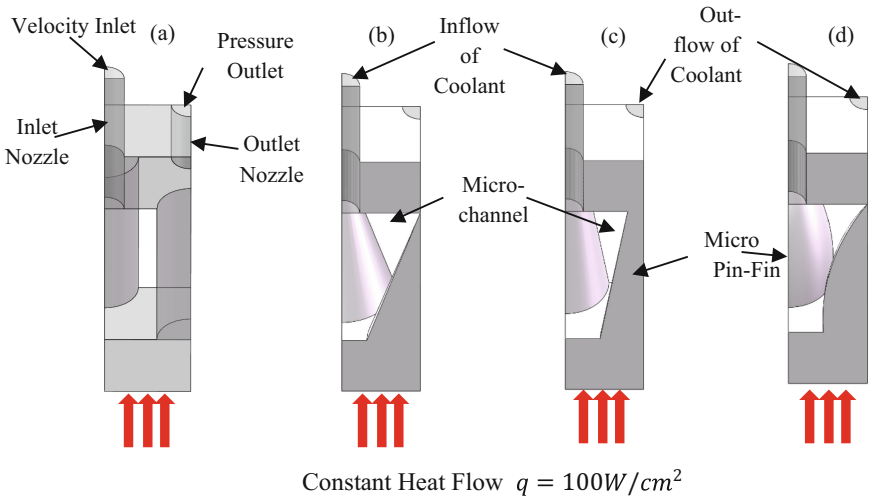

Fig. 1. Schematic representation of the model structure of the heat exchange unit with four micro-pin-fin arrangements. (a) Case A: Cylindrical pin-fins; (b) Case B: Conical pin-fins; (c) Case C: Truncated pin-fins; (d) Case D: Bullet-shaped pin-fins

2.2.2 Governing Equations

According to Ref. [10], when Re < 1000,1000 < Re < 3000, and Re > 3000, the fluid is in laminar, semi-turbulent, and fully turbulent flow for impinging jets, correspondingly. The Reynolds number Re is defined by

$$Re = \frac{\rho v d}{\nu} \tag{2}$$

As the Re in the initial design is 41.806, the flow is in laminar flow. The presence of turbulence creates vortices in the flow region, which in turn enhances the convective heat transfer.

The computational model in this paper is a steady-state adiabatic model without external heat exchange. The coolant is incompressible laminar flow. The fluid-solid-liquid coupling equations are solved by the governing equations, which are the continuity equation, the momentum equation, and the energy equation, as Ref. [4]. The boundary conditions are:

Heating Boundaries:

$$-\lambda_s\left(\frac{\partial T_s}{\partial x_z}\right) = 100W/cm^2 \tag{3}$$

Adiabatic Boundary:

$$-\lambda_s\left(\frac{\partial T_s}{\partial x_z}\right) = 0 \tag{4}$$

Solid-liquid coupling surface

$$-\lambda_s\left(\frac{\partial T_s}{\partial x_z}\right) = h_J\left(T_f - T_0\right) - \lambda_f\left(\frac{\partial T_f}{\partial x_z}\right) \tag{5}$$

Among them, λ_s indicates the thermal conductivity of the solid; T_s and T_f Indicate the temperatures in the solid and liquid regions, correspondingly.

The above governing equations are solved iteratively using the SIMPLE algorithm. The residuals of each governing equation are 10^{-5}, 10^{-5} and 10^{-8}.

According to the mesh independence requirement, we tested three mesh structures. The deviation of pressure drop from Mesh 1 to Mesh 2 is 2.69%. The deviation of pressure drop from Mesh 2 to Mesh 3 is 1.1%. The temperature deviations are all below 0.08%. Thus, Mesh 2 is used for calculation.

3 Results and Discussions

In this section, the effects of constant and variable flow rates in a heat exchange unit composed of four different micro-pin-fin are investigated by numerical simulation methods and the corresponding optimization results.

3.1 Heat Transfer and Fluid Flow

This section analyzes the flow and heat transfer characteristics of four basic examples of heat transfer elements with different micro-pin-fin structures. In this case, the diameter of the nozzle and the micro-pin-fins are at fixed values, and the volumes of micro-pin fins are all created equal. The structural differences of the heat exchange units are mainly reflected in the flow line, flow velocity, temperature, and pressure. Figure 2 shows the velocity distribution and streamline diagrams with four different micro-pin-fin structures. The streamlines of the four models are mainly divided into two directions. One is the flow in the vertical direction of the entrance and exit. Another is the horizontal flow within the microchannel. The streamline of Case A is concentrated in the lower half.

Figure 3 shows the temperature distributions for the four structures. The high-speed jet impacts the thermal boundary layer on the bottom surface, which makes the local thermal boundary layer thinner, increases the temperature gradient, and facilitates heat transfer. The thickness of the thermal boundary layer gradually increases along the direction of cooling liquid flow. The thickest thermal boundary layer is at the hysteresis point below the exit nozzle. Case A and C have sufficient temperature differences and heat exchange areas in the microchannel, and the heat exchange effect is good. Because the bottom boundary layer is too thick and the heat exchange area is small, the base temperature of Case B and Case D is relatively high, and the heat exchange effect is poor. When the flow rate was 0.045 L/min, the maximum temperatures of the substrates of Case A and Case C were 307.14 K and 307.05 K, which were 3.07 K and 2.1 K lower than that of Case B and Case D, respectively.

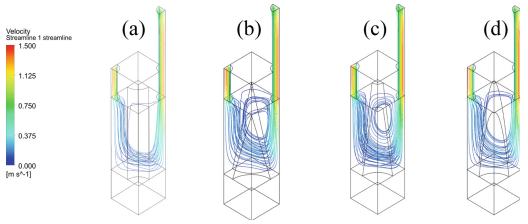

Fig. 2. Distribution of streamlines along the flow direction. (a) Case A: Cylindrical pin-fins; (b) Case B: Conical pin-fins; (c) Case C: Truncated pin-fins; (d) Case D: Bullet-shaped pin-fins

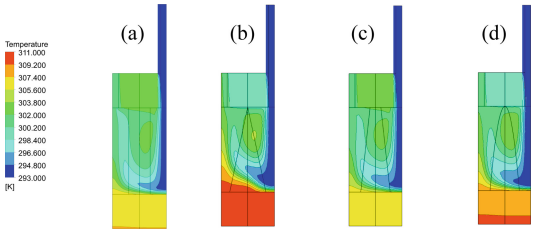

Fig. 3. Temperature profiles along the flow direction. (a) Case A: Cylindrical pin-fins; (b) Case B: Conical pin-fins; (c) Case C: Truncated pin-fins; (d) Case D: Bullet-shaped pin-fins

Figure 4 shows the pressure changes of the heat exchange units with four different structures in the above calculation example. The pressure drop is mainly generated in the nozzle section, while the pressure drop in the microchannel section is lower. From Fig. 4, we see that Case A has a small pressure drop in the microchannel. The remaining three have higher pressure drops within the microchannel. The resulting pressure drop is proportional to the pump work consumed by the system. When the flow rate is 0.045 L/min, the pressure drops of Case A to D are 4824.57 Pa, 5013.23 Pa, 4829.62 Pa, and 4857.31 Pa, respectively, that is, the external power consumed by the conical micro-pin-fin structure for heat exchange most.

The local convective heat transfer coefficients of the heat exchange unit models along the microchannel direction (Y direction) for the four structures are presented in Fig. 5. The local convection heat transfer coefficient is defined as:

$$\overline{h_y} = \frac{T_{W,y} - T_{f,y}}{q_{W,y}} \tag{6}$$

Among them, $q_{W,y}$ is the average heat flow density, $T_{W,y}$ is the average temperature of the solid region on the solid-liquid coupling surface, and $T_{f,y}$ corresponds to the average temperature of the fluid region. The variation of the convective heat transfer coefficient can be roughly divided into three stages: the inlet nozzle part, the microchannel pin-fin part,, and the outlet nozzle part. The high-speed jet improves the heat transfer at the nozzle inlet, resulting in the highest point of convective heat transfer coefficient and the hysteresis point. In the wall-jet region, the coolant flows into the microchannel, and the impingement of the jet decreases. Thus, the convective heat transfer coefficient decreases. The heat transfer of the nozzle exit section is mainly influenced by the micro-pin-fins. This leads to a second hysteresis point in the nozzle exit section. The addition of the micro-pin-fin allows the coolant to maintain a high level of heat transfer over a wide range during flow.

Figure 6 shows the variation of heat transfer coefficient along the vertical Z direction. Thanks to the high-speed wall-jet, the coolant maintains a large convective heat transfer coefficient while flowing through the bottom. As the coolant flows to the outlet nozzle, the influence of the high-speed jet is continuously weakened. Referring to Fig. 2, it can be concluded that the convective heat transfer coefficient remains consistently low level because the coolant flows through Case A with less eddy intensity. Compared to Case A, the bottom flow space of Case B to D is smaller, while the top flow space is larger. Consequently, the convective heat transfer coefficients along the Z-axis in Case B to D increase sharply and are used to compensate for the lower heat exchange due to the lower convective heat transfer coefficient at the bottom.

Figure 7 shows the variation of temperature non-uniformity of heat exchange units with four different structures. To quantify the temperature uniformity, the temperature uniformity index U_{T} is defined as:

$$U_{\mathrm{T}} = \frac{\int_A |\mathrm{T} - \mathrm{T}_{avg}| dA}{\int_A T_{avg} dA} \tag{7}$$

Among them, T and T_{avg} represent the local temperature and the averaged temperature of the underlying surface. Therefore, the uniformity index is lower when the temperature distribution of the heating surface is more uniform. From Fig. 7, we can see

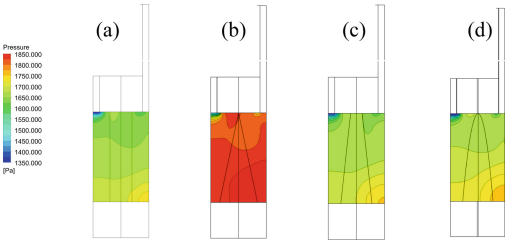

Fig. 4. Pressure contours in microchannels. (a) Case A: Cylindrical pin-fins; (b) Case B: Conical pin-fins; (c) Case C: Truncated pin-fins; (d) Case D: Bullet-shaped pin-fins

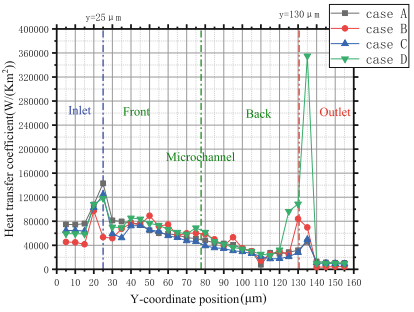

Fig. 5. Local heat transfer coefficient as a function of y-coordinate position.

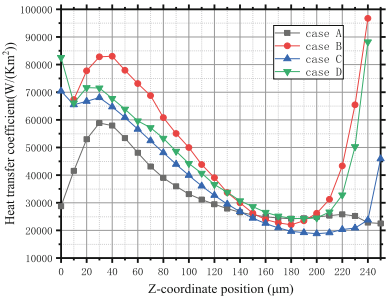

Fig. 6. Local heat transfer coefficient as a function of z-coordinate position.

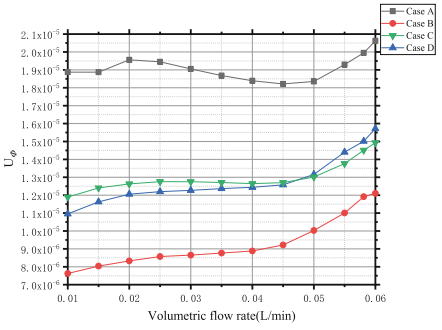

Fig. 7. The effect of temperature unevenness on heat transfer.

that as the flow rate increases, the temperature uniformity index increases, which means that the temperature uniformity increases as well. Case B has the smallest temperature non-uniformity. With the same volume, the bottom surface area of Case B is large and the coolant circulation space is small, thus the thermal conductivity of the bottom surface is better. However, the convective heat transfer effect on the micro-pin-fin surface is poor, and the heat transfer capability of the high-speed jet on the increased heat transfer capacity is restricted to be fully exploited.

3.2 Optimization and Comparison of Variable Flow

Figures 8 show the variation of the thermal resistance as well as the pressure drop with the volume flow rate. The pressure drop increases as the volume flow rate increases from 0.01 L/min to 0.06 L/min. The total thermal resistance is calculated according to the following formula, which is:

$$R_{tot} = \frac{T_{max} - T_{in}}{q} \tag{8}$$

T_{max} indicates the maximum temperature of the bottom surface, T_{in} represents the average surface temperature of the inlet nozzles, and q represents the average heat flow density. It can be easily seen from the figure that the total thermal resistance shows a continuous decline as the flow rate increases. However, the increase in pressure drop reduces the benefit of reducing the total thermal resistance.

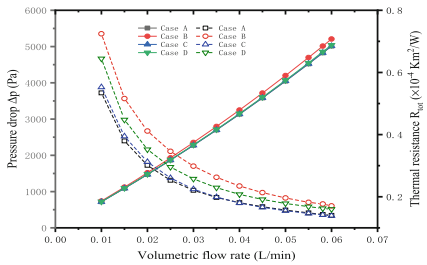

Fig. 8. Trend of total thermal resistance and pressure drop with increasing volume flow.

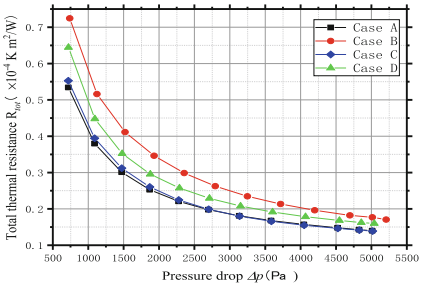

Fig. 9. Plot of total thermal resistance versus pressure drop.

To investigate the correlation between flow rate and heat transfer performance, Fig. 9 depicts the relationship between the total thermal resistance and the change in pressure drop. When the pressure drop is lower than 3000 Pa, Case A has the lowest total thermal resistance when consuming the same amount of pump work. When the power consumption is 2697.98 Pa, the total thermal resistance is reduced to a minimum of 1.97×10^{-5} Km^2/W. When the pressure drop is higher than 3000 Pa, Case C has the smallest thermal resistance under the condition of consuming the same amount of pump work. When the power consumption is 5016.17 Pa, the total thermal resistance is reduced to a minimum of 1.39×10^{-5} Km^2/W.

4 Conclusion

This article presents the pros and cons of the morphologic design of the checkerboard heat sink, including various arrangements of the cylinder, cone, truncated cone, and bullet micro-pin-fins. By changing the structure of the micro-pin-fin and its operating flow rate, this paper assesses its flow and heat transfer performance using thermal resistance and pressure drop, combined with an analysis of the local convective heat transfer coefficient to assist in optimisation. The specific conclusions are as follows.

1. The cylindrical and circular truncated arrangement has superior heat exchange performance and flow properties at the same volume flow rate and the same micro-pin-fin volume.
2. From the point of view of internal flow, the existence of eddy currents is beneficial to convective heat transfer. Therefore, developing eddy current controllability can be used to enhance heat transfer.

References

1. Sahu, V., Joshi, Y.K., Fedorov, A.G.: Hybrid solid state/flfluidic cooling for hot spot removal. Nanoscale Microscale Thermophysical Eng. **13**, 135–150 (2009)
2. Lu, X.Y., et al.: Analysis of heat transfer performance of heat pipe loop for high power LED cooling (in Chinese). Sci China Ser E-Tech Sci **39**, 1944–1998 (2009)
3. Li, B.J., et al.: The implementation of software and hardware for dynamic thermal management of electronic devices (in Chinese). Sci Sin Tech **50**, 1298–1315 (2020)
4. Xu, J., Zhou, T., Xu, X.: Experimental investigation on a novel liquid cooling device for a prismatic Li-ion battery module operating at high ambient temperature. Science China Technol. Sci. **63**(10), 2147–2153 (2020). https://doi.org/10.1007/s11431-020-1605-5
5. Tie, P., et al.: The heat transfer feature of jet impinement cooling for GaN chip (in Chinese). Cryogen Supercond **47**, 55–59 (2019)
6. Gao, X.X., et al.: Simulation study of 3D-ICs with interlayer microchannel liquid cooling (in Chinese). Refrigera Air-Cond **20**, 35–39 (2020)
7. Bello-Ochende, T., Liebenberg, L., Meyer, J.P.: Constructal cooling channels for microchannel heat sinks. Int J Heat Mass Transfer **50**, 4141–4150 (2007)
8. Ju, X., et al.: Numerical investigation of a novel manifold micro-pin-fin heat sink combining chessboard nozzle-jet concept for ultra high heat flux removal. Int J Heat Mass Transfer **126**, 1206–1218 (2018)
9. Shi, Q.L., et al.: Numerical investigation of different nozzle-jet distributions based on chessboard high-topology composite heat sink (in Chinese). Sci Sin Tech **51**, 699–710 (2021)
10. Mcnaughton, K.J., Sinclair, C.G.: Submerged jets in short cylindrical flow vessels. J. Fluid Mech. **25**, 367–375 (1966). https://doi.org/10.1017/S0022112066001708